Journal of Electromagnetic Waves and Applications, Vol. 1, No. 3, 243–267, 1987

The Finite-Difference Time-Domain (FD-TD) Method for Electromagnetic Scattering and Interaction Problems

A. Taflove

Department of Electrical Engineering
and Computer Science
Technological Institute
Northwestern University
Evanston, Illinois 60201, USA

K. R. Umashankar

Communications Laboratory
Department of Electrical Engineering
and Computer Science
University of Illinois at Chicago
Chicago, Illinois 60680, USA

Abstract– This paper summarizes the formulation and recent applications of the finite-difference time-domain (FD-TD) method for numerical modeling of electromagnetic scattering and interaction problems. One of the goals of this paper is to demonstrate that recent advances in FD-TD modeling concepts and software implementation, combined with advances in computer technology, have expanded the scope, accuracy, and speed of FD-TD modeling to the point where it may be the preferred choice for structures that cannot be easily treated by conventional integral equation and asymptotic approaches. As a class, such structures are electrically large, and have complex shapes, material compositions, apertures, and interior cavities. The discussion is highlighted by a succinct review of recent FD-TD modeling validations and research frontiers in radar cross section, coupling to wires and wire bundles in free space and cavities, scattering from surfaces in relativistic motion, inverse scattering, supercomputer and mini-supercomputer software, and radiation condition theory. The paper concludes with a summary of the strong and weak points of FD-TD, and guidelines concerning when FD-TD should (or should not) be applied to high-frequency electromagnetic modeling problems.

INTRODUCTION

Contemporary high-frequency electromagnetic engineering problems can involve wave interactions with complex, electrically-large three-dimensional structures. In the context of this paper, electrically large means objects spanning a number of wavelengths, or equivalently, total phase shifts in the near field substantially exceeding 360°. Electrically complex is used to describe objects having shapes, material compositions, apertures, or interior cavities which produce near fields that cannot be usefully resolved into finite sets of modes or rays. Proper numerical modeling of such near fields requires sampling of the fields at sub-wavelength resolution to avoid aliasing of magnitude and phase information. The goal is to

provide a self-consistent model of the mutual coupling of the electrically-small patches or cells comprising the object.

A candidate numerical modeling approach for this purpose is the finite-difference time-domain (FD-TD) solution of Maxwell's curl equations [1]–[12]. This approach is analogous to existing finite-difference solutions of fluid flow problems encountered in computational aerodynamics, in that the numerical model is based upon a direct solution of the governing partial differential equation. Pursuing this analogy, FD-TD shares the computational requirements of the fluids codes (and other similar large-scale partial differential equation solvers) in terms of computer floating-point arithmetic rate, primary random access memory size, and data bandwidth to secondary memory. Yet, FD-TD is a non-traditional approach to numerical electromagnetic modeling, where frequency-domain approaches have dominated.

One of the goals of this paper is to demonstrate that recent advances in FD-TD modeling concepts and software implementation, combined with advances in computer technology, have expanded the scope, accuracy, and speed of FD-TD modeling to the point where it may be the preferred choice for certain types of scattering and coupling problems. With this in mind, this paper will succinctly review the following recent FD-TD modeling validations and research frontiers:

Scattering: Radar cross section of canonical three-dimensional bodies spanning up to 9 wavelengths [9]–[11];

Penetration and coupling: Plane wave penetration through thin slots having complex paths through thick screens [13], and induced currents excited by an incident plane wave on wires and wire bundles in free space and in a metal cavity [14];

Transient phenomena: Reflection of a plane wave by a relativistically vibrating perfectly-conducting surface [15];

Inverse scattering: Reconstruction of two-dimensional conducting and homogeneous dielectric target shapes from a single-point scattered field pulse response [16];

Supercomputer software: Development of efficient memory management software for the Cray X-MP, and initiation of coarse-grain multi-processing software for the Cray X-MP and Cray-2;

Mini-supercomputer software: Initiation of efficient memory management software for the Floating Point Systems 264, and fine-grained multiprocessing software for the Intel Hypercube; and

Radiation condition theory: Continuation of theoretical work on the theory and application of one-way wave equations [17]–[20], which has already led to the on-surface radiation condition (OSRC) formulation of scattering for convex two-dimensional bodies [21], [22].

GENERAL CHARACTERISTICS OF FD-TD

As stated, FD-TD is a direct solution of Maxwell's time-dependent curl equations. It employs no potentials. Instead, it applies simple, second-order accurate central-

difference approximations [1] for the space and time derivatives of the electric and magnetic fields directly to the respective differential operators of the curl equations. This achieves a sampled-data reduction of the continuous electromagnetic field in a volume of space, over a period of time. Space and time discretizations are selected to bound errors in the sampling process, and to insure numerical stability of the algorithm. Electric and magnetic field components are interleaved in space to permit a natural satisfaction of tangential field continuity conditions at media interfaces. The resulting system of equations for the fields is fully explicit, so that there is no need to set up or solve a set of linear equations, and the required computer storage and running time is proportional to the electrical size of the volume modeled. Overall, the FD-TD marching-in-time procedure results in a simulation of the continuous actual waves by sampled-data numerical analogs propagating in a data space stored in a computer.

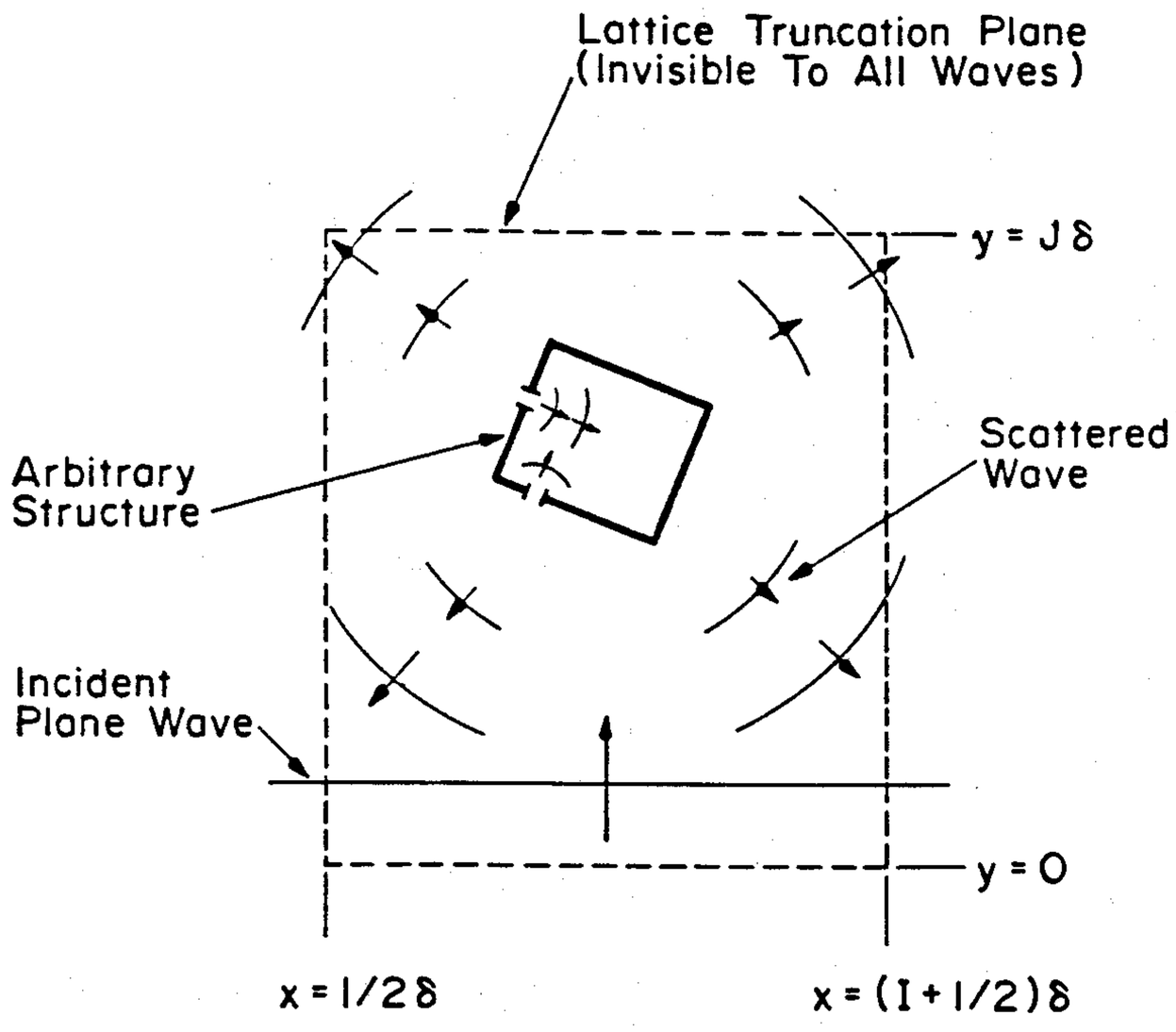

Figure 1. Time-domain wave-tracking concept of the FD-TD method.

Figure 1 illustrates the time-domain wave tracking concept of the FD-TD method. A region of space within the dashed lines is selected for field sampling in space and time. At time $= 0$, it is assumed that all fields within the numerical sampling region are identically zero. An incident plane wave is assumed to enter the sampling region at this point. Propagation of the incident wave is modeled by the commencement of time stepping, which is simply the implementation of the finite-difference analog of the curl equations. Time stepping continues as the

analog of the incident wave strikes the arbitrary structure embedded in the sampling region. All outgoing scattered-wave analogs ideally propagate through the lattice truncation planes with negligible reflection to exit the sampling region. Phenomena such as induction of surface currents, scattering and multiple scattering, penetration through apertures, and cavity excitation are modeled time-step by time-step by the action of the curl equations analog. Self-consistency of these modeled phenomena is generally assured if their spatial and temporal variations are well resolved by the space and time sampling process.

Time stepping is continued until the desired late-time pulse response or steady-state behavior is achieved. An important example of the latter is the sinusoidal steady state, wherein the incident wave is assumed to have a sinusoidal dependence, and time stepping is continued until all fields in the sampling region exhibit sinusoidal repetition.*

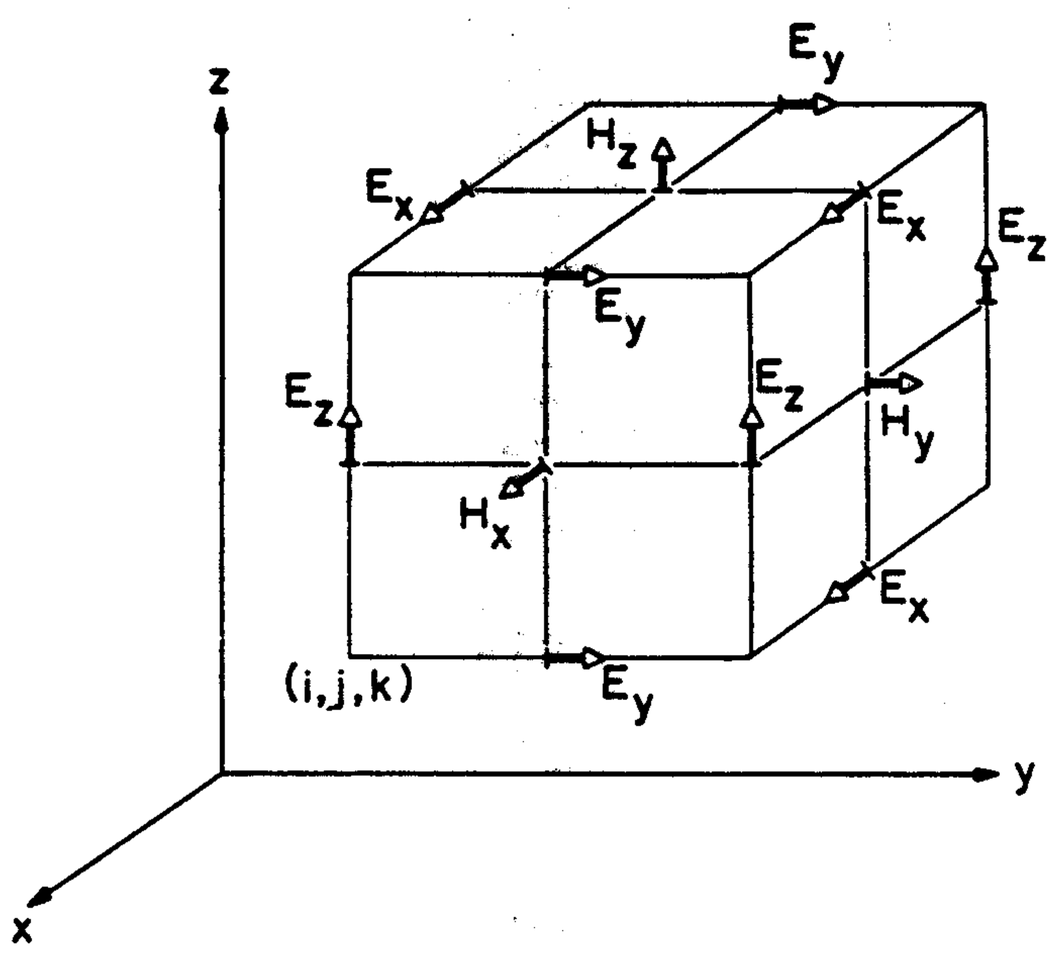

Figure 2. Positions of the field components about a unit cell of the FD-TD lattice.

Figure 2 illustrates the positions of the electric and magnetic field components about a unit cell of the FD-TD lattice in Cartesian coordinates. Note that each magnetic field vector component is surrounded by four circulating electric field vector components, and vice versa. This arrangement permits not only a centered-

---

* Extensive numerical experimentation with FD-TD has shown that the number of complete cycles of the incident wave required to be time-stepped to achieve the sinusoidal steady state is approximately equal to the Q factor of the structure or phenomenon being modeled. A good recent example is the wire/cavity work of [14], reviewed later in this paper.

difference analog to the space derivatives of the curl equations, but also a natural geometry for implementing the integral form of Faraday's Law and Ampere's Law at the space-cell level. This integral interpretation permits a simple but effective modeling of the physics of thin-slot coupling [13], thin-wire coupling [14], and smoothly curved target surfaces [27].

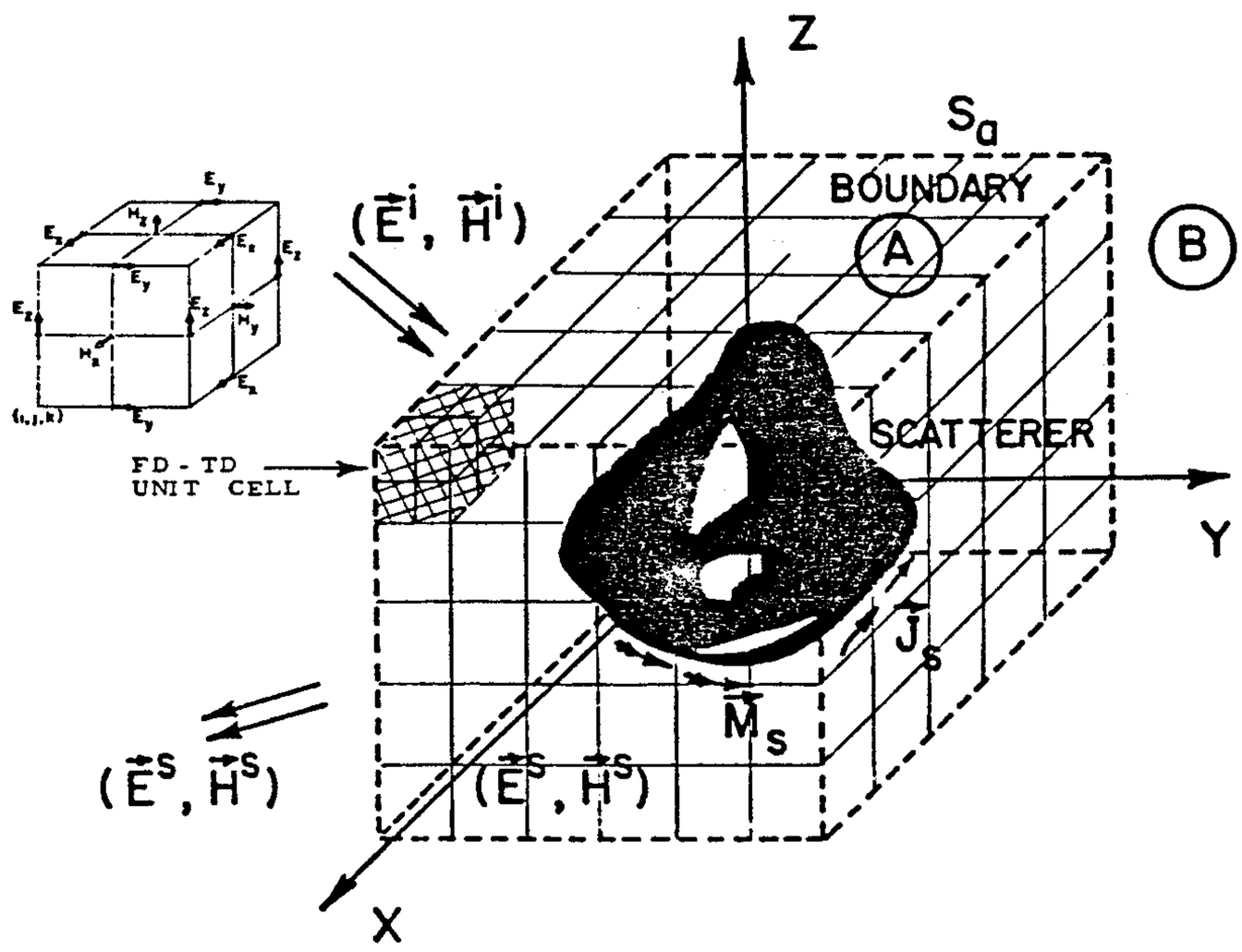

Figure 3. Arbitrary three-dimensional scatterer embedded in a FD-TD space lattice.

Figure 3 illustrates how an arbitrary three-dimensional scatterer is embedded in an FD-TD space lattice comprised of the unit cells of Fig. 2. Simply, desired values of electrical permittivity and conductivity are assigned to each electric field component of the lattice. Correspondingly, desired values of magnetic permeability and equivalent conductivity are assigned to each magnetic field component of the lattice. The media parameters are interpreted by the FD-TD program as local coefficients for the time-stepping algorithm. Specification of media properties in this component-by-component manner results in a stepped-edge, or staircase, approximation of curved surfaces. Continuity of tangential fields is assured at the interface of dissimilar media with this procedure. There is no need for special field matching at media interface points. Stepped-edge approximation of curved surfaces has been found to be adequate in the FD-TD modeling problems studied to date [2], [5], [7], [12], [14]. However, a conformal curved surface approach is being developed to accomodate those problems where surface roughness can

appreciably affect scattering behavior [27].

REVIEW OF FD-TD ALGORITHM DETAILS

Table 1 lists the six coupled equations for the electric and magnetic fields which comprise Maxwell's equations in Cartesian coordinates. Table 2 lists the assumed space/time notation for the field vector components sampled at discrete lattice locations and at discrete time steps. This table also provides the central-difference approximations to the space and time partial derivatives of Maxwell's equations, using the assumed sampled-field notation. Finally, Table 3 provides sample finite-difference time-stepping expressions for a magnetic and an electric field component. As noted earlier, all quantities on the right-hand side of each time-stepping expression are known (stored in computer memory), so that the expressions are fully explicit.

$$\frac{\partial H_x}{\partial t} = \frac{1}{\mu}\left(\frac{\partial E_y}{\partial z} - \frac{\partial E_z}{\partial y}\right) \tag{1a}$$

$$\frac{\partial H_y}{\partial t} = \frac{1}{\mu}\left(\frac{\partial E_z}{\partial x} - \frac{\partial E_x}{\partial z}\right) \tag{1b}$$

$$\frac{\partial H_z}{\partial t} = \frac{1}{\mu}\left(\frac{\partial E_x}{\partial y} - \frac{\partial E_y}{\partial x}\right) \tag{1c}$$

$$\frac{\partial E_x}{\partial t} = \frac{1}{\epsilon}\left(\frac{\partial H_z}{\partial y} - \frac{\partial H_y}{\partial z} - \sigma E_x\right) \tag{1d}$$

$$\frac{\partial E_y}{\partial t} = \frac{1}{\epsilon}\left(\frac{\partial H_x}{\partial z} - \frac{\partial H_z}{\partial x} - \sigma E_y\right) \tag{1e}$$

$$\frac{\partial E_z}{\partial t} = \frac{1}{\epsilon}\left(\frac{\partial H_y}{\partial x} - \frac{\partial H_x}{\partial y} - \sigma E_z\right) \tag{1f}$$

Table 1. Maxwell's curl equations in Cartesian coordinates.

$$(i, j, k) = (i\delta, j\delta, k\delta) \tag{2a}$$

$$F^n(i, j, k) = F(i\delta, j\delta, k\delta, n\delta t) \tag{2b}$$

$$\frac{\partial F^n(i, j, k)}{\partial x} = \frac{F^n(i + 1/2, j, k) - F^n(i - 1/2, j, k)}{\delta} + O(\delta^2) \tag{3a}$$

$$\frac{\partial F^n(i, j, k)}{\partial t} = \frac{F^{n+1/2}(i, j, k) - F^{n-1/2}(i, j, k)}{\delta t} + O(\delta t^2) \tag{3b}$$

Table 2. Central-difference approximations to space and time partial derivatives.

$$H_x^{n+1/2}(i,j+1/2,k+1/2) = H_x^{n-1/2}(i,j+1/2,k+1/2) + \frac{\delta t}{\mu(i,j+1/2,k+1/2)\delta} \cdot [E_y^n(i,j+1/2,k+1) - E_y^n(i,j+1/2,k) + E_z^n(i,j,k+1/2) - E_z^n(i,j+1,k+1/2)] \tag{4a}$$

$$E_z^{n+1}(i,j,k+1/2) = \frac{1-\frac{\sigma(i,j,k+1/2)\delta t}{2\epsilon(i,j,k+1/2)}}{1+\frac{\sigma(i,j,k+1/2)\delta t}{2\epsilon(i,j,k+1/2)}} \cdot E_z^n(i,j,k+1/2) + \frac{\delta t}{\epsilon(i,j,k+1/2)\delta} \cdot \frac{1}{1+\frac{\sigma(i,j,k+1/2)\delta t}{2\epsilon(i,j,k+1/2)}} \cdot [H_y^{n+1/2}(i+1/2,j,k+1/2) - H_y^{n+1/2}(i-1/2,j,k+1/2) + H_x^{n+1/2}(i,j-1/2,k+1/2) - H_x^{n+1/2}(i,j+1/2,k+1/2)] \tag{4b}$$

Table 3. Examples of finite-difference expressions for field components derivatives.

The choice of δ and δt is motivated by reasons of accuracy and algorithm stability, respectively. To insure the accuracy of the computed spatial derivatives of the electromagnetic fields, δ must be small compared to a wavelength. $\delta \leq \lambda/10$ is sufficient to realize less than $\pm 7\%$ uncertainty (± 0.6 dB) of the FD-TD solution of near fields due to the approximation of the spatial derivatives [11]. For $\delta \leq \lambda/20$, this uncertainty drops to less than $\pm 2\%$ ($\pm 0.2\ dB$). δ should also be small enough to permit resolution of principal surfaces and/or volumetric details of the structure modeled.

To insure the stability of the time-stepping algorithm exemplified by (4*a*) and (4*b*), δt is chosen to satisfy the inequality [2]

$$\delta t \leq \left(\frac{1}{\delta x^2} + \frac{1}{\delta y^2} + \frac{1}{\delta z^2}\right)^{-\frac{1}{2}} \quad c_{\max}^{-1} \leq \frac{\delta}{c_{\max}\sqrt{3}} \qquad \text{(for a cubic lattice)} \tag{5}$$

where $c_{\max}$ is the maximum wave phase velocity within the model. Note that the corresponding stability criterion set forth in Eqs. (7) and (8) of Reference [1] is incorrect [2].

Figure 4 illustrates the division of the FD-TD lattice into total-field and scattered-field regions. This division has been found to be very useful since it permits the simulation of an incident plane wave in the total-field region with arbitrary angle of incidence and polarization [8], [20]. Three additional important benefits arise from this lattice division. First, a large near-field computational dynamic range is achieved, since the scatterer of interest is embedded in the total-field region. Thus, low field levels in shadow regions or within cavities are

computed directly without suffering subtraction noise (as would be the case if scattered fields in such regions were time-stepped via FD-TD, and then added to the incident field to obtain the low total-field levels). Second, embedding the scatterer in the total-field region permits a natural satisfaction of tangential field continuity across media interfaces, as discussed earlier, without having to compute the incident field at possibly numerous points along complex, scatterer-specific loci. The arrangement of Fig. 4 requires computation of the incident field only along the fixed, regular connecting surface between the total-field and scattered-field regions to permit generation of the incident wave in the total-field region [8], [20].

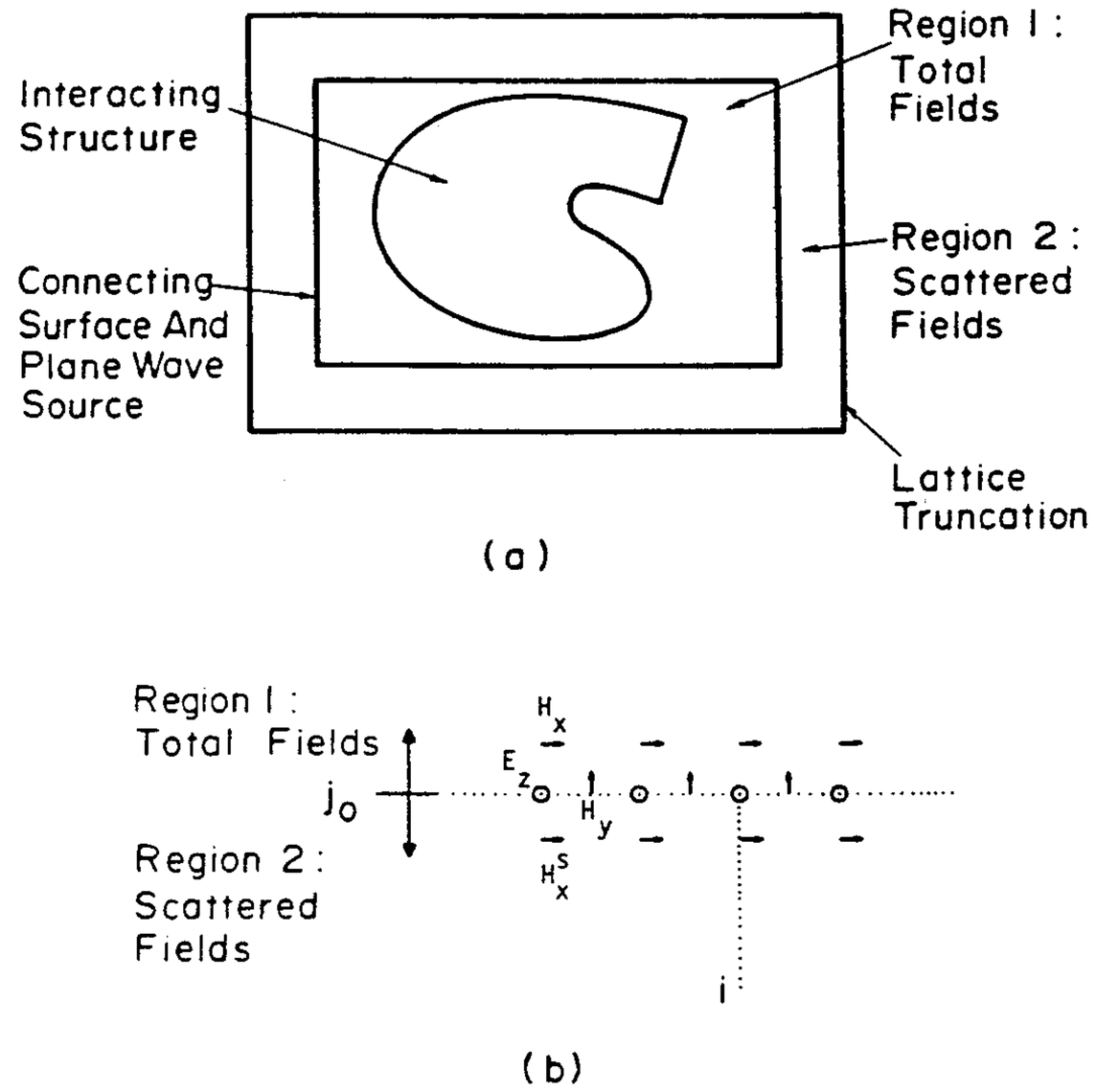

Figure 4. Division of FD-TD lattice into total-field and scattered-field regions: (a) Lattice division; (b) Fields at connecting plane $y = j_0\delta$.

Third, the provision of a well-defined scattered-field region in the FD-TD lattice permits the near-to-far field transformation illustrated in Fig. 5. The dashed virtual surface shown in Fig. 5 can be located along convenient lattice planes in the scattered field region of Fig. 4. Tangential scattered fields computed via FD-TD at this virtual surface can then be weighted by the free-space Green's function and then summed to provide the far-field response and radar cross section [8]–[11].

Figure 4 uses the term "lattice truncation" to designate the outermost lattice planes in the scattered field region. The fields at these planes cannot be computed using the centered-differencing approach discussed earlier because of the assumed absence of known field data at points outside of the lattice truncation. These data are needed to form the central differences. Therefore, an auxiliary lattice truncation condition is necessary. This condition must be consistent with Maxwell's equations in that an outgoing scattered-wave analog striking the lattice truncation must exit the lattice without appreciable non-physical reflection, just as if the lattice truncation was invisible. It has been shown that the required lattice truncation condition is really a radiation condition in the near field [17]–[20]. Further, it has been shown that convenient local approximations of the exact radiation condition can be generated and applied with good results [8]–[11], [17]–[20]. The procedure for constructing more precise local approximations of the exact radiation condition is now understood [17]–[19]. These approximations are currently under study for numerical implementation in the FD-TD computer programs.

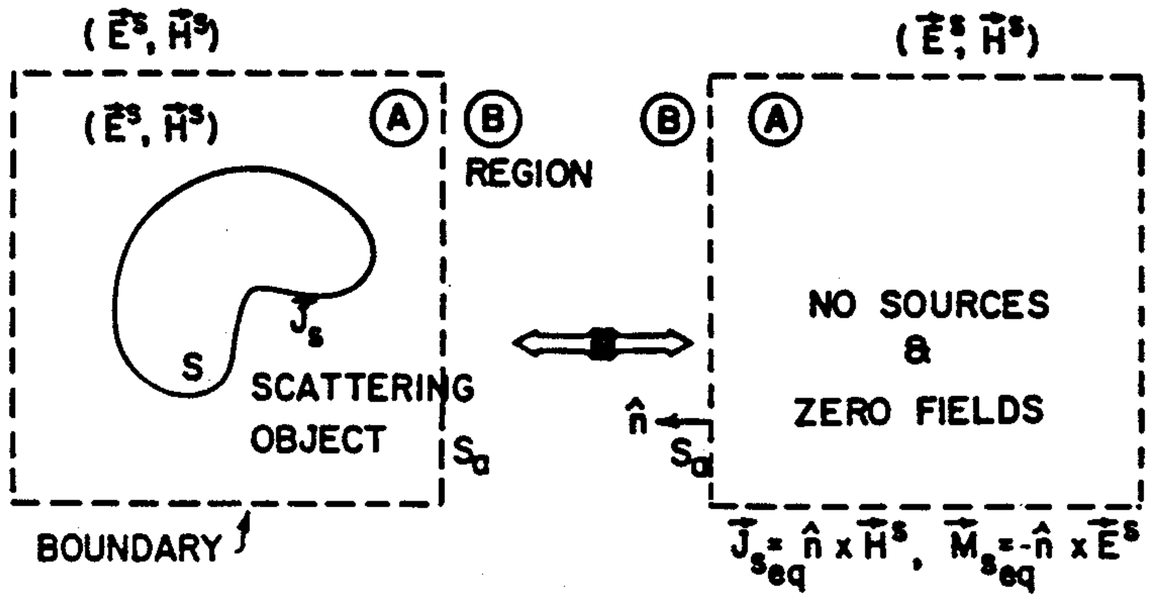

Figure 5. Near-to-far field transformation geometry: (a) original problem; (b) equivalent problem external to the virtual surface S_a.

EXAMPLES OF RECENT FD-TD MODELING VALIDATIONS

Scattering and Radar Cross Section

Analytical and experimental validations have been obtained relative to FD-TD modeling of canonical three-dimensional conducting bodies spanning 1/3 to 9 wavelengths [9]–[11]. For brevity, only one such validation will be reviewed here.

Figure 6 depicts the geometry of a crossed-plate scatterer comprised of two

flat plates electrically bonded together to form the shape of a "T". The main plate has the dimensions 30 cm × 10 cm × 0.33 cm, and the bisecting fin has the dimensions 10 cm × 10 cm × 0.33 cm. The illumination is a plane wave at 0° elevation angle and TE polarization relative to the main plate, and at the frequency 9.0 GHz. (Thus, the main plate spans 9.0 wavelengths in this model.)

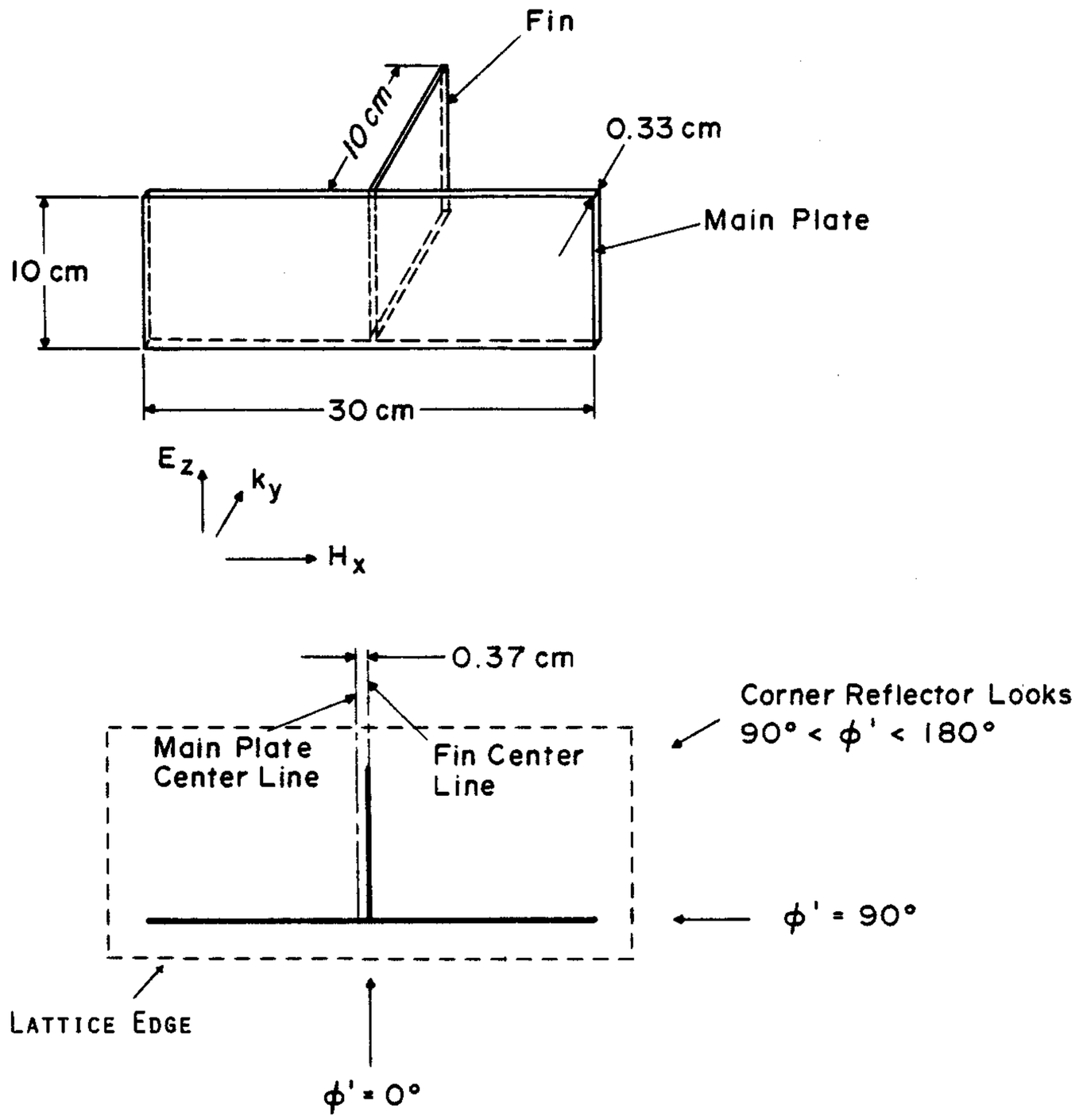

Figure 6. Geometry of crossed-plate (T) scatterer and illumination.

Note that look angle azimuths between 90° and 180° provide substantial corner reflector physics, in addition to the edge diffraction, corner diffraction, and other effects found for an isolated flat plate. For the 9-GHz FD-TD model, the lattice cell size is 0.3125 cm, approximately 1/11 wavelength. The main plate is formed by $32 \times 96 \times 1$ cells; the bisecting fin is formed by $32 \times 32 \times 1$ cells; and the overall lattice is comprised of $48 \times 112 \times 48$ cells (1,548,288 unknown field components). Note that the lattice truncations are located *only 8 cells* from the scatterer's main plate and fin edges. The slightly eccentric positioning of the bisecting fin is accounted for in the FD-TD model. 661 time steps are used, equivalent to 31 cycles of the incident wave at 9 GHz.

Measurements of the radar cross section (RCS) versus look angle azimuth were performed in the anechoic chamber facility operated by SRI International, Menlo Park, CA. Figure 7 compares the FD-TD predictions with the SRI measurements. It is seen that the agreement is within about 1 dB over a total RCS-pattern dynamic range of 40 dB. Locations of peaks and nulls of the pattern are accurately predicted to within $1°$. Note especially the excellent agreement for look angle azimuths greater than $90°$, where there is a pronounced corner-reflector effect. As stated in [10], it appears that this case (and similar 9-wavelength cases studied) represents the largest detailed three-dimensional numerical scattering models of any type ever verified wherein a uniformly fine spatial resolution and the ability to treat nonmetallic composition is incorporated in the model.

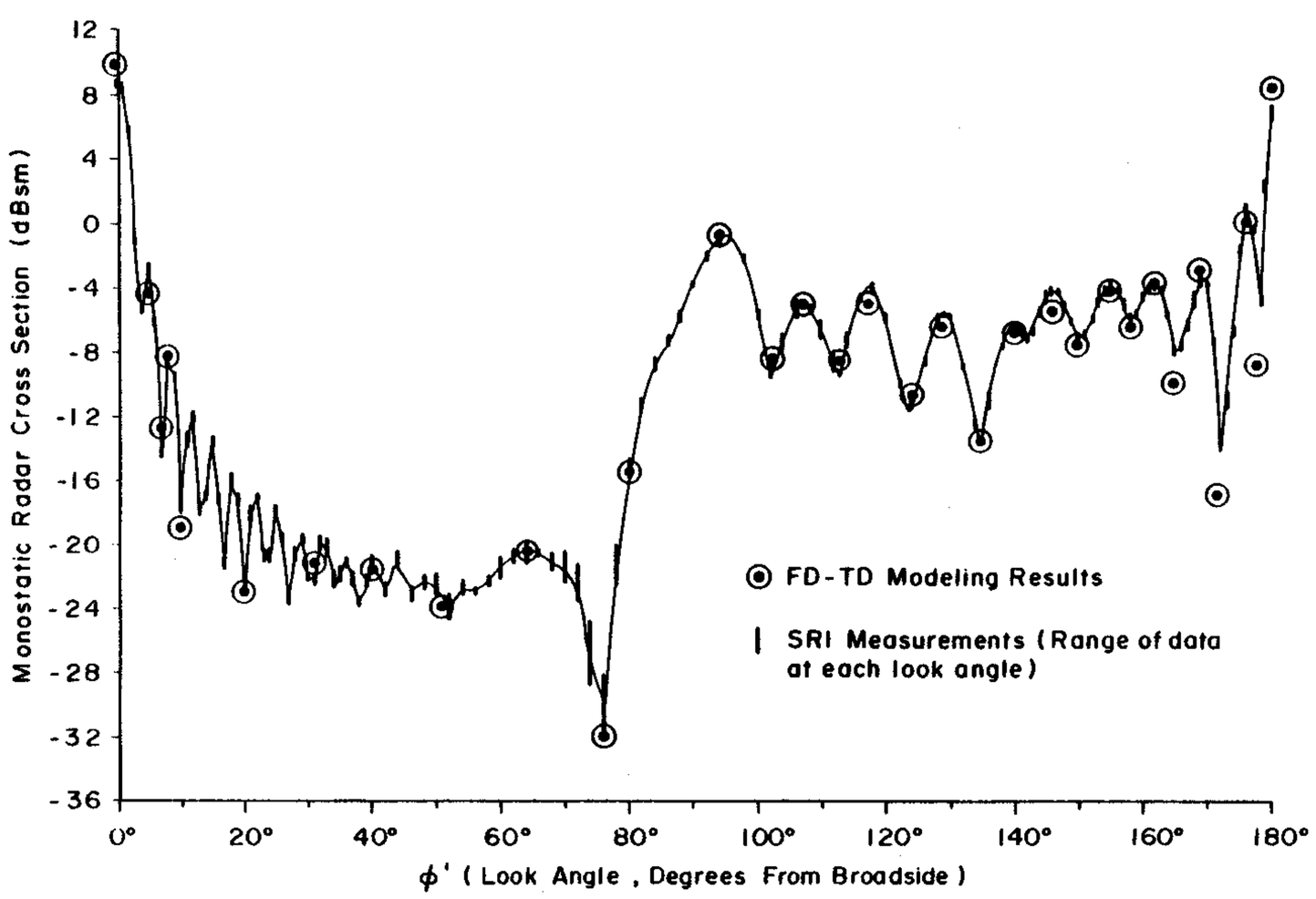

Figure 7. Comparison of FD-TD modeling predictions with SRI measurements for the crossed-plate scatterer at 9 GHz (maximum scatterer size $= 9\lambda_0$).

Wave Penetration and Coupling

Analytical and/or experimental validations have been obtained relative to FD-TD modeling of plane wave penetration through thin slots having complex paths through thick screens [13], and induced currents excited by an incident plane wave on wires and wire bundles in free space and in a metal cavity [14]. For brevity, selected validations are reviewed here only for the wire coupling problem.

Figure 8 shows the analytical validation results for the induced currents on a bundle comprised of four wires, where three are of equal length. Here, a wire

of length 0.6 m is assumed at the center of the bundle, and three parallel wires of length 0.3 m are assumed to be located at 120° separations on a concentric circle of diameter 0.01 m. The radii of all wires in the bundle are equal, and set to 0.001 m. The assumed excitation is in free space, provided by a 1-GHz, TM-polarized, plane wave at normal incidence to the bundle.

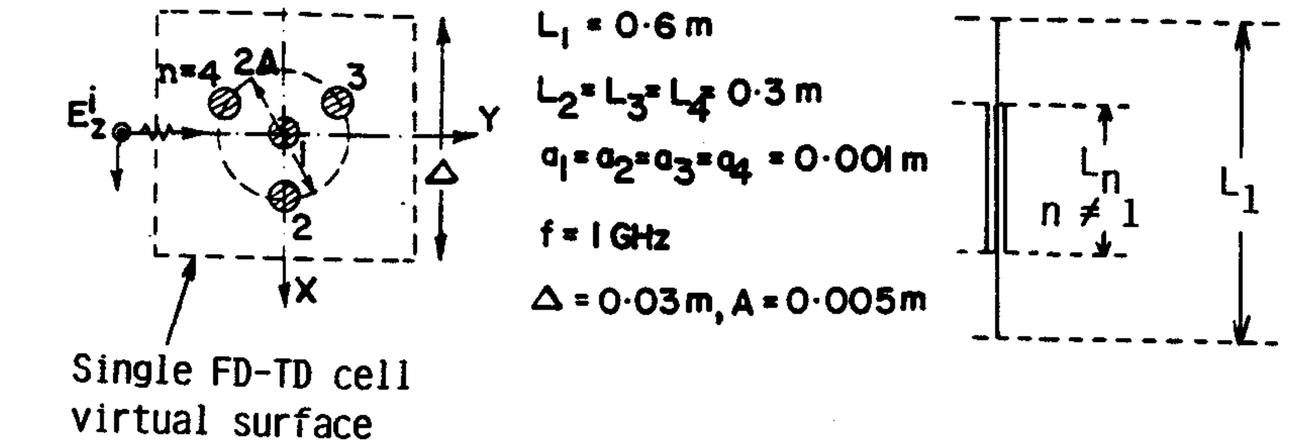

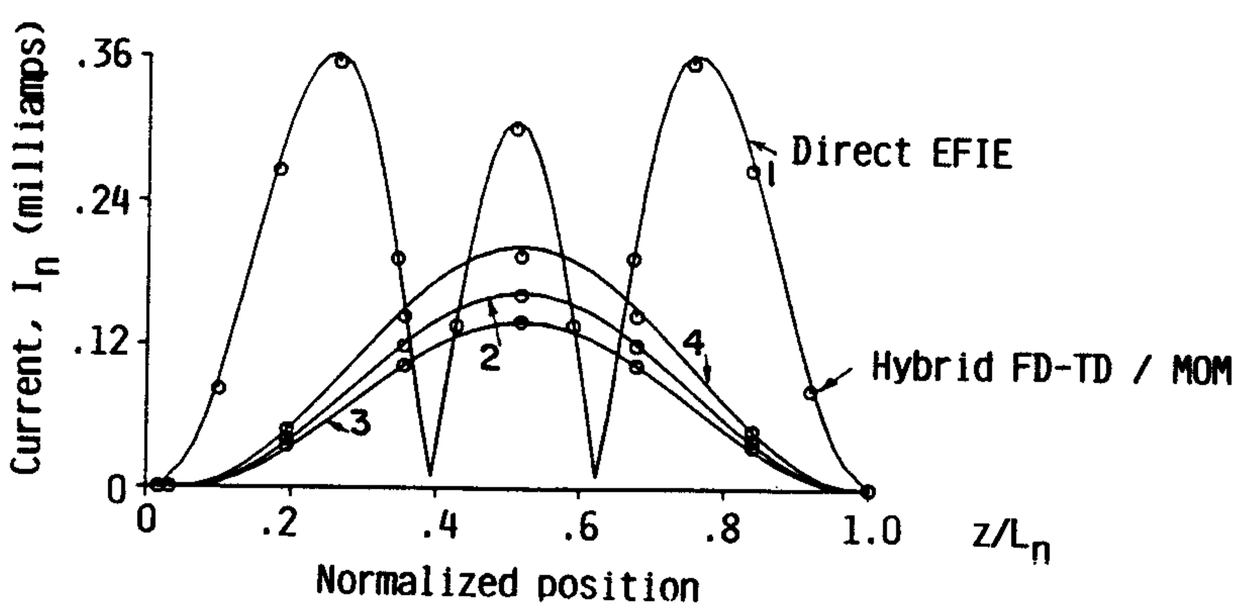

Figure 8. Comparison of hybrid FD-TD/MOM modeling predictions with direct EFIE for induced currents on a wire bundle illuminated by a plane wave in free space.

For purposes of FD-TD modeling, the bundle is embedded within a $16 \times 16 \times 36$ cell space lattice, which allows 8 cells between the bundle and the lattice truncation planes. A uniform cell size of 0.03 m (1/10 wavelength) is employed. Note that the cross section of the bundle fits into a single FD-TD cell. Following the technique of [14], the bundle is replaced by a single wire having varying equiva-

lent radius corresponding to the three sections along the bundle axis. (Here, the two outer sections are of length 0.15 m and have a radius of 0.001 m; while the middle section is of length 0.3 m and has an equivalent radius of 0.003347 m.) The physics of the single wire of varying equivalent radius is incorporated in the FD-TD model by using a Faraday's Law contour integral model for the looping magnetic field components adjacent to the wire [14]. The FD-TD model is time-stepped to 30 cycles to obtain convergence of the tangential fields at a virtual surface conveniently located at the cell boundary containing the equivalent wire (shown as a dashed line in Fig. 8). These fields are then utilized as excitation to obtain the currents induced on the individual wires of the original bundle. This last step is performed by setting up an electric field integral equation (EFIE), and solving via the method of moments (MOM). Figure 8 shows an excellent correspondence between the results of the hybrid FD-TD/MOM procedure described above and the usual direct EFIE solution for the induced current distribution on each wire of the bundle. In this figure, note that the horizontal axis represents normalized position along each wire, so that each current distribution extends between 0.0 and 1.0, despite the differing actual wire lengths.

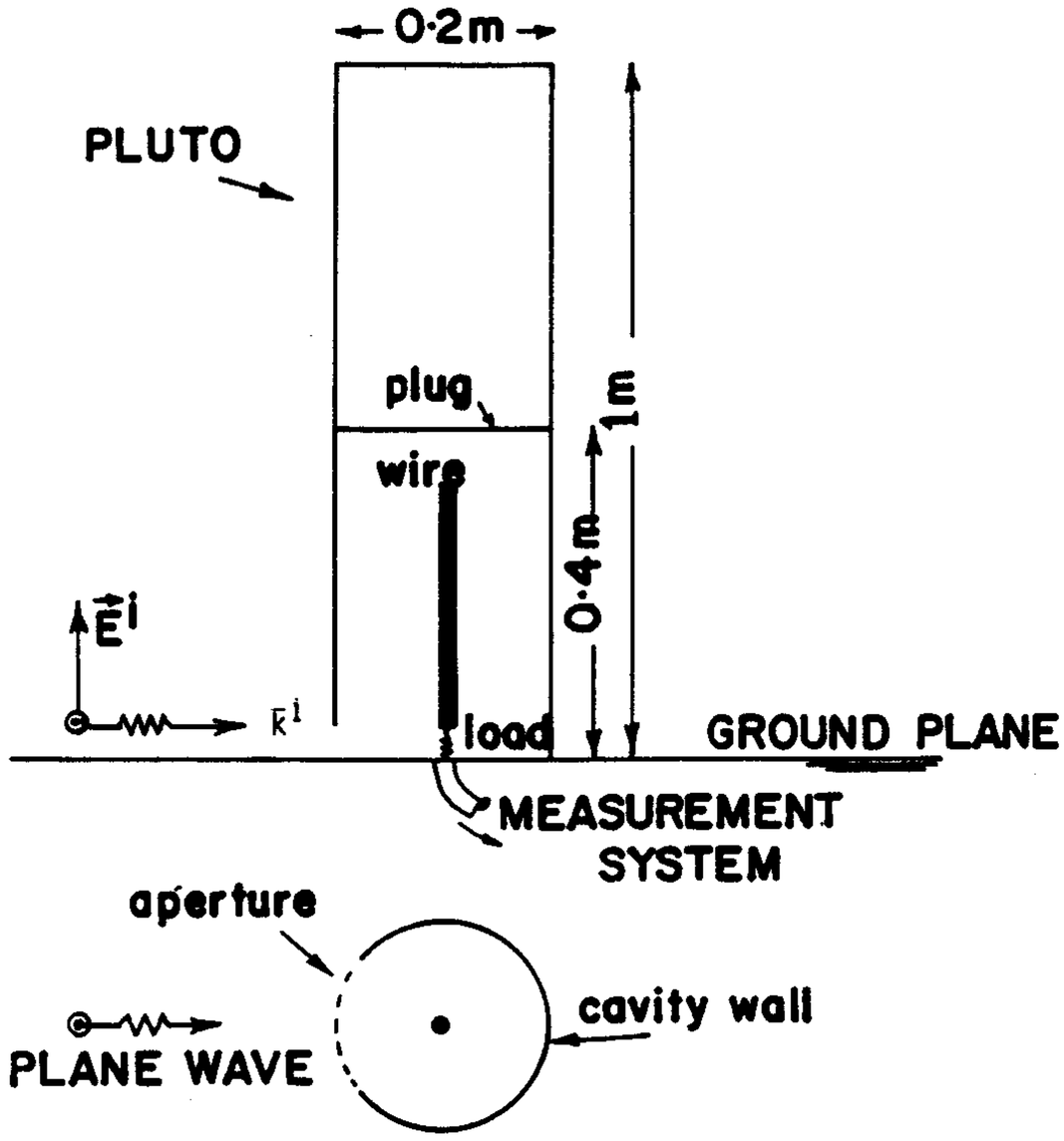

Figure 9. Pluto experimental geometry.

We next consider the experimental validation of the hybrid FD-TD/MOM model summarized above for the case of one and two wires within a metal cavity. Specifically, the experimental setup employed is the PLUTO (Preliminary Livermore Universal Test Object), shown in Fig. 9 [23,24]. PLUTO is a 1.0 m high,

0.20 m diameter, cylindrical metal can above a ground plane. Approximate plane wave excitation is provided by an electrically-large conical monopole referenced to the same ground plane. The aperture, usually a circumferential slot at the ground plane, has an adjustable size. Other adjustments include the position of the internal shorting plug and the position and number of the internal wires. For the cases studied, the circumferential slot aperture has 0.125 m arc length and 0.0125 m gap. The internal shorting plug is 0.40 m above the ground plane. For the one-wire study, a wire of length 0.30 m and radius 0.0004953 m is centered within PLUTO and connected to the ground plane with a lumped 50-ohm load. For the two-wire study, parallel wires of these dimensions are located 0.01 m apart at the center of PLUTO. Here, one of the wires is shorted to the ground plane, and one is connected to the ground plane with a lumped 50-ohm load. Measured data includes the magnitude and phase of the transfer function between the incident electric field and the voltage across the wire load over a wide range of UHF and microwave frequencies. The frequency range discussed here is 1.0 to 1.25 GHz, which includes a prominent coupling peak apparently due to the slot resonance.

For purposes of FD-TD modeling, PLUTO is embedded within a 16 x 32 x 88 cell space lattice. Even symmetry in both the z and x directions is exploited to minimize computer resources. Extensive convergence studies indicate that the stepped-surface FD-TD approximation of the smooth PLUTO cylinder wall and circumferential slot aperture provides a loading effect which shifts the computed resonant coupling peak downward in frequency from the measured value. It is found that the bulk of this downward shift is caused by the stepped-surface approximation of the aperture, and that this frequency-shift component can be eliminated by employing a Faraday's Law contour integral model to reduce the total stepped-edge length of the aperture to the desired value of 0.125 m [14]. With δ =0.0125m (1/24 wavelength at 1.0 GHz), the residual downward shift in the coupling peak is about 32 MHz (2.8%) for the single-wire case, and about 18 MHz (1.6%) for the two-wire case. To permit a straightforward comparison of the modeled and measured coupling response with this residual frequency shift eliminated, the lattice cell size is reduced by 2.8% (to 0.012144m) and 1.6% (to 0.0123m) for the two cases.

Figures 10(a) and 10(b) compare (as a function of frequency) the measured and numerically modeled wire load current for the one-wire and two-wire cases, respectively, assuming a 1 v/m incident electric field. With the small residual resonance frequency shift eliminated, excellent agreement is observed for both cases. Note that the two-wire case is an especially challenging test of the hybrid FD-TD/MOM model, since the observed Q factor of the coupling response, defined as the center frequency divided by the half-power bandwidth, is high (approximately 75). Indeed, it is found that the FD-TD code has to be stepped through as many as 80 cycles to approximately reach the sinusoidal steady state for excitation frequencies near the resonant peak. However, substantially fewer cycles of time stepping are needed away from the resonance, as indicated in the figure.

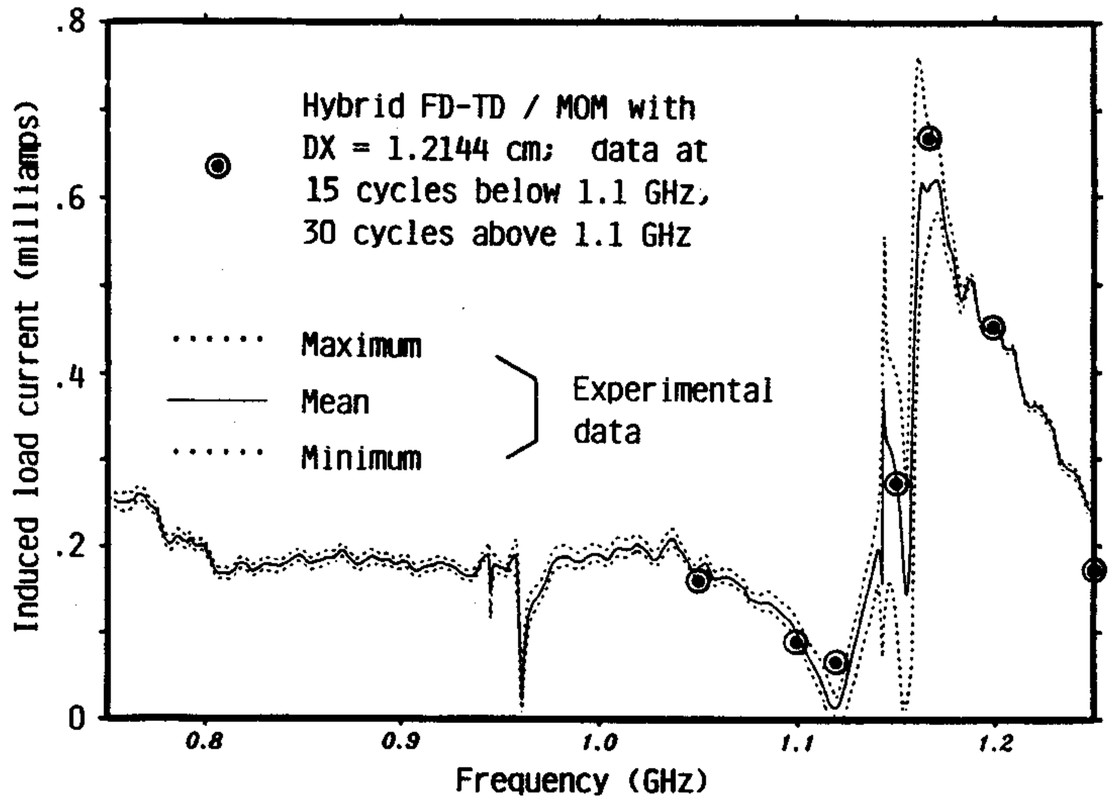

(a)

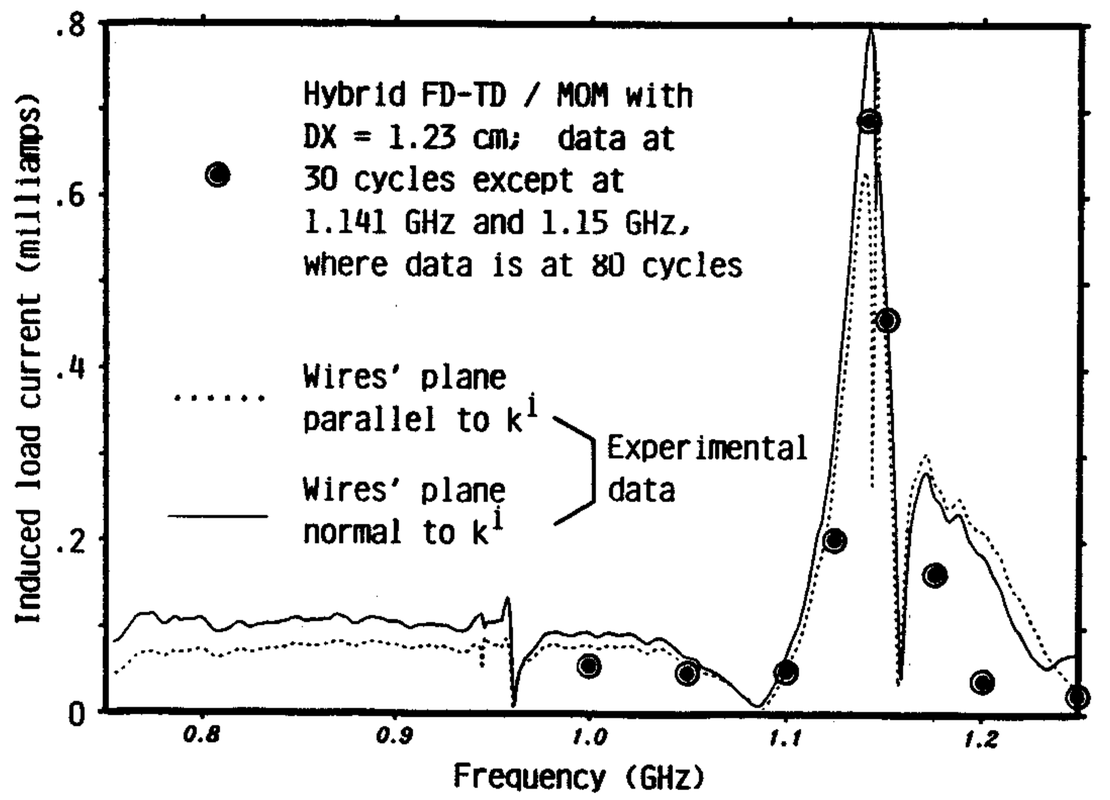

(b)

Figure 10. Comparison between experimental data and calculation based on hybrid FD-TD/MOM technique: (a) single wire in cavity, (b) two wires in cavity.

Figures 11(a) and 11(b) show the predicted detailed distribution of the induced currents on the single wire and on each of the wires of the two-wire bundle in PLUTO at their respective resonant peaks (1.166 GHz and 1.141 GHz). Only the current at the base of each wire is experimentally verified, as in Figs. 10(a) and 10(b). Figures 11(a) and 11(b) are included since little data has been published concerning coupling to wires in three-dimensional cavities.

The hybrid FD-TD/MOM approach introduced in [14] and reviewed here ap-

pears to have substantial promise for allowing the numerical modeling of electromagnetic coupling to realistic wires and cables within complex cavities. This approach takes advantage of the detailed volumetric modeling afforded by FD-TD, and the detailed wire modeling afforded by MOM, by modeling the cavity physics and wire bundle physics in a self-consistent manner.

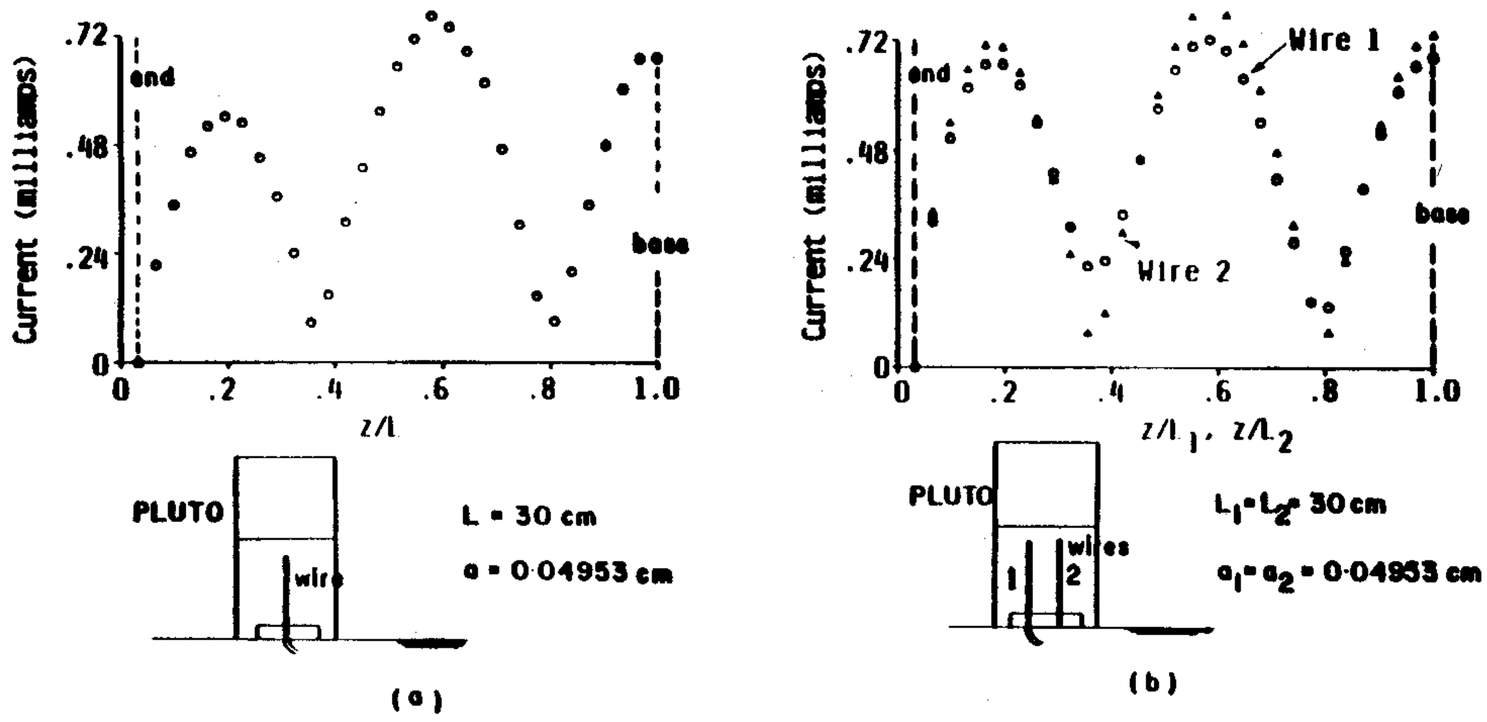

Figure 11. Distribution of induced currents on the wire(s) in Pluto predicted by the hybrid FD-TD/MOM model at the resonant frequency of the coupling response: (a) single wire case; (b) two wire bundle case.

Transient Phenomena

Analytical validations have been obtained relative to FD-TD modeling of reflection of a monochromatic plane wave by a perfectly-conducting surface either moving at a uniform relativistic velocity or vibrating at a frequency and amplitude large enough so that the surface attains relativistic speeds [15]. The latter case will be summarized here.

Figure 12(a) depicts the geometry of the vibrating surface and its illumination. FD-TD modeling is performed as usual, with the addition of a fully relativistic field boundary condition at the surface, and linear interpolation is used to compute the incident field at the surface when its position does not coincide with a field sample point [15]. Figure 12(b) graphs the predictions of the moving-boundary FD-TD code for the magnitude of the spectral component of the reflected wave at the illumination frequency as a function of the maximum surface speed normalized to the speed of light. For this case, the surface vibration frequency is fixed at one-fifth of the illumination frequency. (It should be noted that the vibrating surface generates a spectrum similar to tone-modulated FM, with spectral components below, at, and above the illumination frequency at sideband frequencies equal to integer multiples of the vibration frequency.) An analysis available in the literature [25] demonstrates that the magnitude of the reflected field at the

illumination frequency has a Bessel function (order zero) dependence upon the normalized maximum surface speed. This dependence is also graphed in Fig. 12(b) to permit comparison with the FD-TD results. We see that there exists an excellent correspondence between the numerical and analytical results.

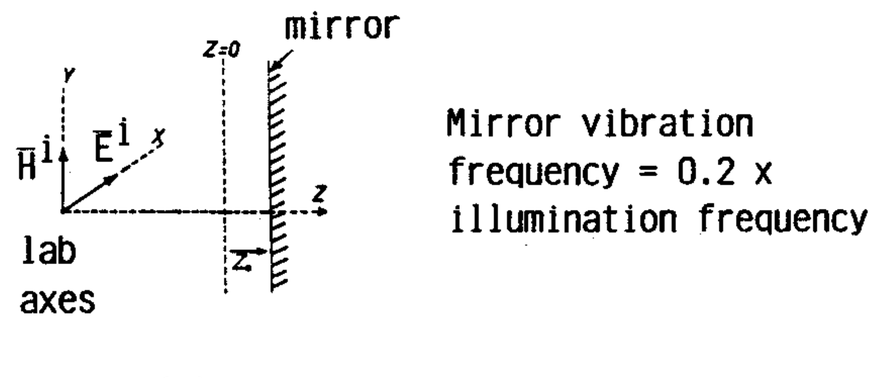

(a)

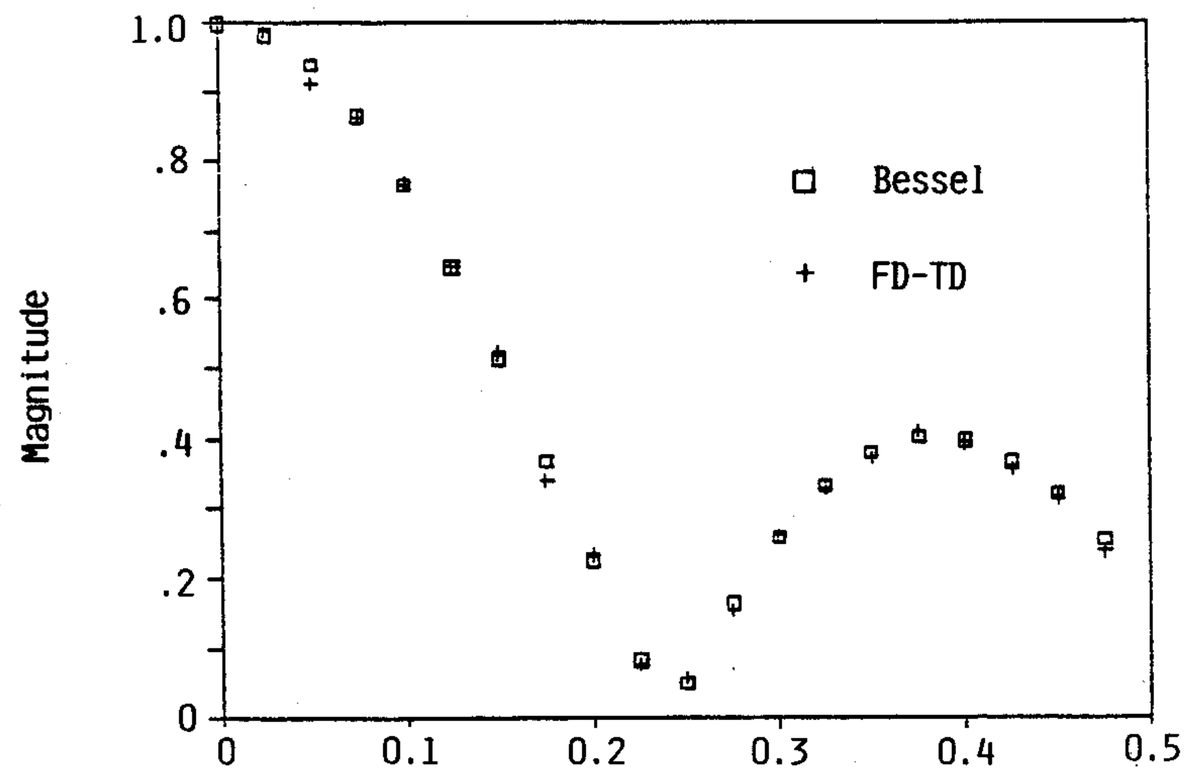

(b)

Figure 12. Magnitude of reflected field at the illumination frequency as a function of maximum surface speed: (a) geometry; (b) Bessel (analytical) vs. FD-TD.

The moving-boundary FD-TD code is currently being adapted to model even more complex time-variable phenomena. In all such cases, the time domain formulation of FD-TD is of prime importance since it permits us to deal with rapidly time-variable phenomena in a natural way.

Inverse Scattering

Initial work has demonstrated the possibility of accurately reconstructing the shape of a two-dimensional conducting or homogeneous dielectric target from its scattered field pulse response observed at only a *single point.** The general approach involves setting up a numerical feedback loop which uses a two-dimensional FD-TD code as a forward-scattering element, and a specially constructed nonlinear optimization code as the feedback element. FD-TD generates a test pulse response for a proposed target shape. The test pulse is compared to the measured pulse, and an error signal is developed. Working on this error signal, the nonlinear optimization element perturbs the originally proposed target shape in a manner to drive down the error. Upon repeated iterations, the proposed target shape ideally converges to the actual shape [16], a strategy similar to that of [26].

The advantage of working in the time domain is that a target shape can be reconstructed sequentially in time as the incident pulse moves across the target, taking advantage of causality. This reduces the complexity of reconstruction since only a portion of the target shape is being generated at each iteration.

For a conducting target, detailed reconstruction begins by locating the point on the target whose response to the incident pulse is first sensed at the observation point. The FD-TD lattice points adjacent to the initial point are then perturbed by sequentially assigning them high values of conductivity. The new addition to the target surface is obtained by comparing the scattered electric field values (observed at a single point) for each perturbation with the measured values, and selecting the surface perturbation that gives the best agreement with measured data in the least-squares sense. This process is repeated using the target surface points generated in the previous iteration as the base from which to launch the new surface perturbation. In this manner, the actual target surface contour is generated synchronously as the leading edge of the incident pulse moves across the target.

The FD-TD/feedback technique has been successfully used to accurately reconstruct conducting and homogeneous dielectric target shapes such as triangles, rectangles, and J-shapes [16]. Currently, the "measured" input data is generated by a high-resolution forward FD-TD code for a half-sine incident pulse, and reconstruction is accomplished with a coarser resolution FD-TD code in the numerical feedback loop. Figure 13 illustrates (to scale) one such reconstruction, a prism having a 0.6×0.3 wavelength triangular cross section reconstructed from simulated measured data taken at a single point 15 wavelengths away. Efforts are now underway to obtain actual measured data for such two-dimensional targets. Preliminary indications are that measurement errors and noise may primarily affect reconstruction of the target shape in shadow regions. Simulated signal-to-noise ratios as low as 30 dB, however, have been found to permit exact reconstructions of 1-wavelength size targets in a number of cases [16].

---

* Extension of this two-dimensional work to full three-dimensional configurations involves issues of uniqueness not currently addressed.

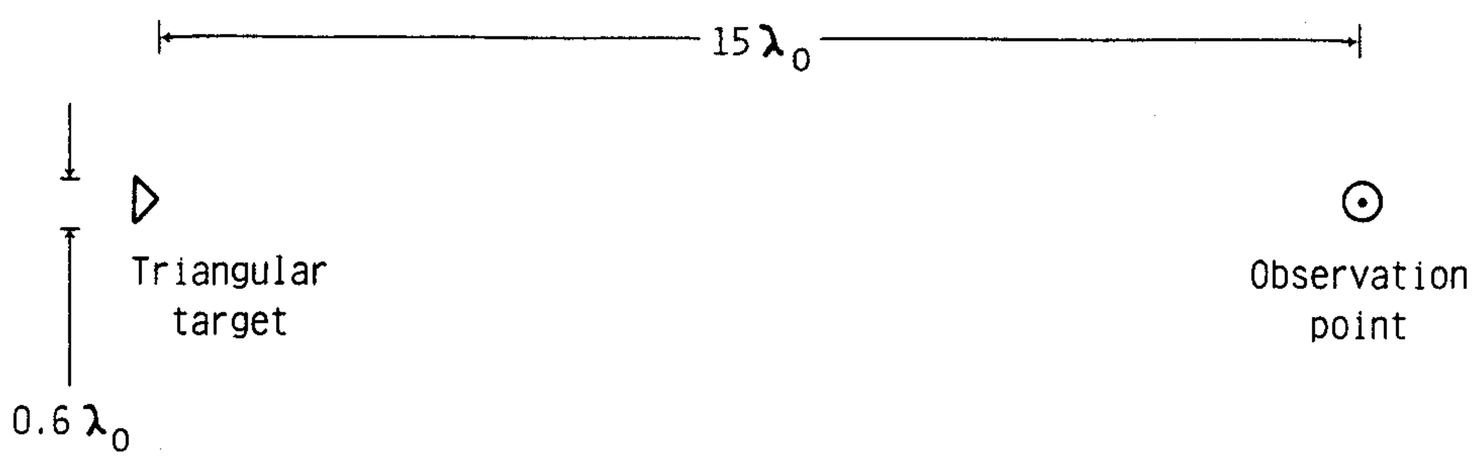

Figure 13. Relative scale of one FD-TD/feedback inverse scattering target reconstruction.

AVDANCES IN FD-TD SOFTWARE

Supercomputer Software

Let us now consider computation times of present FD-TD codes. Table 4 lists computation times (derived either from benchmark runs or based on analysts' estimates) for modeling one look angle of a 10-wavelength three-dimensional scatterer using the present FD-TD code. Four computing systems are listed in the table. The first is the Digital Equipment VAX 11/780, without floating point accelerator. The second and third are, respectively, single-processor and four-processor versions of the Cray-2. The fourth is a hypothetical next-generation machine operating at an average rate of 10 Gflops (10-billion floating point operations per second). This last computer is generally expected to be available about 1990.

Table 4. Computation times.

Machine	10-Wavelength Model Present FD-TD Code *
VAX 11/780 (no floating point accelerator)	40.0 h
Cray-2 (single processor, using the VAX Fortran)	12.0 min
Cray-2 (single processor, some code optimization)	3.0 min
Cray-2 (four processors, some code optimization)	1.0 min (est.)
True 10 Gflop machine (Available around 1990)	2.0 sec (est.)

* 1.55×10^6 unknown field components, 661 time steps.

Note that the single-processor Cray-2, using the VAX code with no modifications, reduces the FD-TD modeling time by 200:1. With some code modifications

to take advantage of features specific to the single-processor Cray-2, the reduction in modeling time is 800:1. With the use of all four processors of the Cray-2, it is estimated that the reduction in modeling time would be 2400:1. Clearly, it is advantageous to run existing FD-TD software on the Cray-2 (or similar machines), rather than the VAX. Further, optimization of FD-TD software for such supercomputers will likely lead to additional time-savings benefits.

The recent availability of supercomputers such as the Cray X-MP and Cray-2 to university researchers via programs sponsored by National Science Foundation has permitted substantial progress to be made in FD-TD code applications and optimization. For example, efficient memory management FD-TD software for the single-processor Cray X-MP has recently been finished and validated. This software can intelligently map a very large electromagnetic field data base onto the Cray solid-state device (SSD) which is used as the secondary memory for the X-MP. Efficient interleaving of field data in transverse lattice planes and the use of asynchronous input/output calls contribute to the realization of a nearly balanced code (equal time devoted to arithmetic and data input/output). Work is now being initiated to develop coarse-grain multiprocessing FD-TD software for the Cray X-MP and Cray-2 to take advantage of the availability of up to four highly capable processors on each machine.

Mini-Supercomputer Software

It is acknowledged that many individuals wishing to utilize FD-TD to model large electromagnetics problems will not have access to Cray-class supercomputers. Therefore, research has been initiated to develop software for machines of much lower cost which can have capabilities comparable to the original Cray-1. As a class, these machines have been termed mini-supercomputers.

Two widely different computers of this type are now being studied. The first is the Floating Point Systems 264, which is considered to be a vector array processor. Here, the recently completed memory management FD-TD software for the single-processor Cray X-MP has been adapted, since the Floating Point Systems machine can suffer from the same bottleneck problem of data input/output to secondary memory for large modeling runs. This bottleneck would cause much or most of the arithmetic speed of the computer to be lost since data calls would dominate running time.

The second mini-supercomputer being studied is the Intel Hypercube D-5. This computer has 32 microprocessors reconfigurable via software command to have a number of modes of connectivity, such as rings, trees, nearest-neighbor grids, and full hypercube. In operation, each microprocessor can be assigned a specific part of the FD-TD lattice, and all can work in parallel. (The Hypercube is an example of a broad class of moderately-to-massively parallel architectures recently introduced.) Here, the goal is to gain experience with the fine grain multiprocessing software required for such a machine, and to develop and validate a FD-TD code.

RADIATION CONDITION THEORY

One outgrowth of an increasing understanding of wave physics modeled via differential marching-in-time approaches has been the advance of the theory of one-way wave equations [17]–[20]. One-way wave equations yield radiation conditions which can truncate a FD-TD lattice in the near field and in the time domain with acceptably small non-physical wave reflections, as discussed earlier. Theoretical work in this area is being continued to further improve FD-TD radiation conditions to permit models of structures with large RCS dynamic range.

An interesting spin-off of the work on radiation condition theory has been the recent introduction of the on-surface radiation condition (OSRC) formulation of scattering for convex two-dimensional bodies [21], [22]. OSRC was prompted by the observation that FD-TD radiation boundary surfaces could be brought very close to a scatterer (refer to the crossed-plate RCS model discussed earlier) with completely acceptable far-field results. It was conjectured that applying a suitable radiation boundary condition even closer to a scatterer could permit an approximation for the near-surface fields which could serve as a zero-order guess in an iterative procedure. A surprising result was obtained by accident: namely, if the radiation boundary condition were applied directly on the scatterer surface, the original integral equation for the scattered field could be reduced to merely a line integral of known fields around the surface contour (for the TM case) or an ordinary differential equation to be solved around the surface contour (for the TE case). Note that FD-TD is no longer involved. Numerical experiments with OSRC for circular cylinders, square cylinders, and flat strips, indicate substantial promise for this new approach as a useful alternative to present integral equation and uniform asymptotic methods for electrically-large, convex, two-dimensional structures. Research is also being directed to better understand why OSRC works as well as it does.

SUMMARY OF THE CHARACTERISTICS OF FD-TD

This section will concisely list the strong points and limitations of FD-TD, the types of problems FD-TD is suited for and why, when FD-TD should be used, and when FD-TD should not be used.

Strong Points of FD-TD

1. FD-TD can provide volumetric models of structures (possibly with complicated cavities) spanning 10 or more wavelengths in three dimensions, and yet maintain a uniform space resolution of 1/10 wavelength. FD-TD accuracy in calculating near and far fields is generally within ± 1 dB.
2. FD-TD has a dimensionally-low computer storage and running time proportional to N, the number of electromagnetic field unknowns in the volume modeled. FD-TD models with $N \sim 10^6$ are currently routine. Conventional detailed numerical modeling approaches such as the method of moments (MOM) have an N^2 to N^3 dependence, limiting applicability to $N < 10^3$, in general.
3. The explicit formulation of FD-TD is excellent for programming on modern

vectorizing and multiprocessing computers.
4. FD-TD can easily interface with other detailed numerical modeling approaches such as the method of moments, when desirable.

Limitations of FD-TD

1. The FD-TD code must be re-run when the incident wave angle is changed.
2. Present FD-TD codes staircase smooth surfaces. (This limitation is disappearing, however, as new versions of the FD-TD codes employ contour-integral conformal smooth surface models [27].)
3. The discrete FD-TD space lattice causes dispersion of propagating pulses in two and three dimensions.
4. Supercomputer usage is presently advised for large three-dimensional problems. Such machines may not be available to the general user.

Types of Problems FD-TD is Suited for, and Why

1. FD-TD is suited for modeling complex metal and dielectric structures, including cavities, for wave penetration, coupling, and radar cross section. This is because it achieves fine spatial resolution, naturally satisfies field continuity conditions at media interfaces, computes fields at every lattice point within the structure, and permits an easy derivation of far fields from near fields.
2. FD-TD is suited for modeling coupling to wires and wire bundles in free space or in cavities. This is because it can incorporate field singularities near wires, and can interface with MOM to provide a self-consistent treatment of wires and bundles in complicated exposure environments.
3. FD-TD is suited for modeling wave interactions with non-linear media and rapidly time-varying media. This is because non-linearities and rapid time-dependent behavior can be naturally modeled by a time-domain approach.
4. Within the limits set by lattice dispersion effects, FD-TD can model the pulse response of scatterers, because it is a direct time-domain approach.

FD-TD Should Be Used When:

1. The structure to be modeled has an extremely complex surface shape and/or internal structure.
2. The structure to be modeled spans more than 2–5 wavelengths in each of the three dimensions.
3. The number of electromagnetic field unknowns to be solved is greater than 5,000-10,000.
4. The problem involves pulse response, non-linearities, or time-varying media which mandate a detailed time-domain solution.

FD-TD Should Not Be Used When:

1. The structure to be modeled has only a moderately complex surface shape, no internal structure, and requires fewer than 1,000 field unknowns to be solved, thus permitting the application of MOM.
2. The structure is highly conducting, electrically large, and has no important

re-entrant features, thus permitting the application of the geometric theory of diffraction (GTD) or its variants to model scattering.
3. The structure's scattering is dominated by rough-surface physics, eliminating the effective use of staircase approximation of curved surfaces. (New versions of the FD-TD codes will not have this problem.)
4. There is available a less computationally-intensive approach which provides the needed data.

ACKNOWLEDGMENTS

The authors wish to acknowledge the research contributions of their colleague, Prof. G. A. Kriegsmann of Northwestern University, and their graduate students at Northwestern and the Unversity of Illinois at Chicago. The authors also wish to acknowledge the support of their sponsors, including Lawrence Livermore National Laboratory (Contract No. 6599805); NASA Lewis Research Center (Grant No. NAG 3-635), and National Science Foundation (Grant No. ECS-8515777).

The Editor thanks R. C. Chou, D. Dudley, C. Lee, M. Tsuk, and one anonymous Reviewer for reviewing the paper.

REFERENCES

1. Yee, K. S., "Numerical solution of initial boundary value problems involving Maxwell's equations in isotropic media," *IEEE Trans. Antennas Propagat.,* Vol. AP–14, 302–307, May 1966.
2. Taflove, A., and M. E. Brodwin, "Numerical solution of steady-state electromagnetic scattering problems using the time-dependent Maxwell's equations," *IEEE Trans. Microwave Theory Tech.,* Vol. MTT–23, 623–630, Aug. 1975.
3. Taflove, A., and M. E. Brodwin, "Computation of the electromagnetic fields and induced temperatures within a model of the microwave-irradiated human eye," *IEEE Trans. Microwave Theory Tech.,* Vol. MTT–23, 888–896, Nov. 1975.
4. Holland, R., "Threde: A free-field EMP coupling and scattering code," *IEEE Trans. Nuclear Sci.,* Vol. NS–24, 2416–2421, Dec. 1977.
5. Kunz, K. S., and K. M. Lee, "A three-dimensional finite-difference solution of the external response of an aircraft to a complex transient EM environment: Part I — The method and its implementation," *IEEE Trans. Electromagn. Compat.,* Vol. EMC–20, 328–333, May 1978.
6. Meriwether, D. E., R. Fisher, and F. W. Smith, "On implementing a numeric Huygens' source scheme in a finite-difference program to illuminate scattering bodies," *IEEE Trans. Nuclear Sc.,* Vol. NS–27, 1819–1833, Dec. 1980.
7. Taflove, A., and K. R. Umashankar, "A hybrid moment method/finite-difference time-domain approach to electromagnetic coupling and aperture penetration into complex geometries," *IEEE Trans. Antennas Propagat.,* Vol. AP–30, 617–627, July 1982.
8. Umashankar, K. R., and A. Taflove, "A novel method to analyze electromagnetic scattering of complex objects," *IEEE Trans. Electromagn. Compat.,* Vol. EMC–24, 397–405, Nov. 1982.
9. Taflove, A., and K. R. Umashankar, "Radar cross section of general three-dimensional scatterers," *IEEE Trans. Electromagn. Compat.,* Vol. EMC–25, 433–440, Nov. 1983.
10. Taflove, A., K. R. Umashankar, and T. G. Jurgens, "Validation of FD-TD modeling of the radar cross section of three-dimensional structures spanning up to nine

wavelengths," *IEEE Trans. Antennas Propagat.,* Vol. AP–33, 662–666, June 1985.
11. Umashankar, K. R., and A. Taflove, "Analytical models for electromagnetic scattering," Air Force Contract F19628-82-C-0140, Electromagn. Sci. Division, Rome Air Development Center, Hanscom AFB, MA, Final Rep., June 1984.
12. Sullivan, D. M., D. T. Borup, and O. P. Gandhi, "Use of the finite-difference time-domain method in calculating EM absorption in human tissues," *IEEE Trans. Biomed. Engrg.,* Vol. BME–34, 148–157, Feb. 1987.
13. Taflove, A., K. R. Umashankar, B. Beker, F. Harfoush, and K. S. Yee, "Detailed FD-TD analysis of electromagnetic fields penetrating narrow slots and lapped joints in thick conducting screens," accepted by *IEEE Trans. Antennas Propagat.,* to be published in late 1987.
14. Umashankar, K. R., A. Taflove, B. Beker, and K. S. Yee, "Calculation and experimental validation of induced currents on coupled wires in an arbitrary shaped cavity," accepted by *IEEE Trans. Antennas Propagat.,* to be published in late 1987.
15. Harfoush, F., A. Taflove, and G. A. Kriegsmann, "FD-TD analysis of electromagnetic wave scattering from relativistically moving surfaces," submitted to *IEEE Trans. Antennas Propagat.,* Oct. 1986.
16. Strickel, M. A., A. Taflove, and K. R. Umashankar, "Accurate reconstruction of two-dimensional conducting and homogeneous dielectric target shapes from a single-point TM scattered field pulse response," submitted to *IEEE Trans. Antennas Propagat.,* Feb. 1987.
17. Engquist, B., and A. Majda, "Absorbing boundary conditions for the numerical simulation of waves," *Math. Comp.,* Vol. 31, 629–651, July 1977.
18. Kriegsmann, G. A., and C. Morawetz, "Solving the Helmholtz equation for exterior problems with variable index of refraction: I," *SIAM J. Sci. Stat. Comput.,* Vol. 1, 371–385, Sept. 1980.
19. Bayliss, A., and E. Turkel, "Radiation boundary conditions for wave-like equations," *Commun. Pure Appl. Math.,* Vol. 33, 707–725, 1980.
20. Mur, G., "Absorbing boundary conditions for the finite-difference approximation of the time-domain electromagnetic field equations," *IEEE Trans. Electromagn. Compat.,* Vol. EMC–23, 377–382, Nov. 1981.
21. Kriegsmann, G. A., A. Taflove, and K. R. Umashankar, "A new formulation of electromagnetic wave scattering using an on-surface radiation boundary condition approach," *IEEE Trans. Antennas Propagat.,* Vol. AP–35, 153–161, Feb. 1987.
22. Umashankar, K. R., A. Taflove, and G. A. Kriegsmann, "Extension of on-surface radiation condition theory to scattering by two-dimensional homogeneous dielectric objects," *Proc. 1986 URSI Radio Science Meeting,* Philadelphia, PA, 158, June 1986.
23. King, R. J., J. K. Breakall, H. G. Hudson, J. J. Morrison, V. G. McGevna, K. S. Kunz, A. P. Ludwigsen, and D. K. Gnade, "Phenomenology of microwave coupling, Part I," UCID-20215, Lawrence Livermore National Laboratory, Livermore, CA 94550, Nov. 1984.
24. King, R. J., A. P. Ludwigsen, and K. S. Kunz, "Phenomenology of microwave coupling, Part II," UCID-20215 Part 2, Lawrence Livermore National Laboratory, Livermore, CA 94550, Aug. 1985.
25. Van Bladel, J., *Relativity and Engineering.* Springer-Verlag, New York, 1984.
26. Bennett, C. L., and G. F. Ross, "Time-domain electromagnetics and its applications," *Proc. IEEE ,* Vol. 66, 299–318, March 1978.
27. Jurgens, T. G., A. Taflove, and K. R. Umashankar, "FD-TD conformal modeling of smooth curved surfaces," presented at URSI Radio Science Meeting, Blacksburg, VA, June 1987.

Allen Taflove was born in Chicago, IL on June 14, 1949. He received the B.S., M.S., and Ph.D. degrees in electrical engineering from Northwestern University, Evanston, IL, in 1971, 1972, and 1975, respectively. From 1975 to 1984, he was a staff member at IIT Research Institute in Chicago, IL, holding the positions of Associate Engineer, Research Engineer, and Senior Engineer. In 1984, he joined the Department of Electrical Engineering and Computer Science at Northwestern University, Evanston, IL, as an Associate Professor. Since then, he has developed several research programs in the area of computational electromagnetics. His current interests include applications of recent supercomputers, wave penetration and scattering by large, complex structures, inverse scattering/target synthesis, and the new on-surface radiation condition theory.

Korada R. Umashankar received the B.E. degree from Mysore University, India, in 1962; the M.E. degree from the Indian Institute of Science, Bangalore, India, in 1964; and the Ph.D. degree from the University of Mississippi, University, MS, in 1974; all in electrical engineering. From 1964 to 1969, he was Assistant Professor and Head of the Department of Electrical Engineering, College of Engineering, Karnatak University, Hubli, India. During 1974 and 1975, he was a Postdoctoral Research Associate, and from 1975 to 1977, Assistant Professor of Electrical Engineering at the University of Mississippi. From 1977 to 1979, he was the National Research Council Visiting Fellow at the U.S. Air Force Weapons Laboratory, Kirtland AFB, NM. During 1979 to 1984, he was Senior Engineer at IIT Research Institute, Chicago, IL. Currently, he is Associate Professor of Electrical Engineering and Computer Science at the University of Illinois at Chicago, Chicago, IL. His primary research work is in the development of analytical and numerical techniques in electromagnetic theory, EMP/EMC interactions, and EM simulation studies.